Evaluation of the Difference in the Rate Coefficients of F2 + NOx (X = 1 or 2) → F + FNOx by the Stereochemical Arrangement Using the Density Functional Theory.

ARTICLE *in* THE JOURNAL OF PHYSICAL CHEMISTRY A · JANUARY 2015

Impact Factor: 2.69 · DOI: 10.1021/jp510886b · Source: PubMed

3 AUTHORS, INCLUDING:

Satomi Tajima

Toyota Central R & D Labs., Inc.

26 PUBLICATIONS **147** CITATIONS

SEE PROFILE

Toshio Hayashi

Nagoya University

67 PUBLICATIONS **366** CITATIONS

SEE PROFILE

THE JOURNAL OF PHYSICAL CHEMISTRY A

Article

pubs.acs.org/JPCA

Evaluation of the Difference in the Rate Coefficients of $F_2 + NO_x$ ($x = 1$ or 2) → $F + FNO_x$ by the Stereochemical Arrangement Using the Density Functional Theory

Satomi Tajima,* Toshio Hayashi, and Masaru Hori

Plasma Nanotechnology Research Center (PLANT), Graduate School of Engineering, Nagoya University, Furo-cho, Chikusa-ku, Nagoya, Aichi, Japan 464-8603

ABSTRACT: The rate coefficient of $F_2 + NO \rightarrow F + FNO$ is 2 to 5 orders of magnitude higher than that of $F_2 + NO_2 \rightarrow F + FNO_2$ even though bond energies of FNO and FNO_2 only differ by ~0.2 eV. To understand the cause of having different rate coefficients of these two reactions, the change in total energies was calculated by varying the stereochemical arrangement of F_2 with respect to NO_x ($x = 1$ or 2) by the density functional theory (DFT), using CAM-B3LYP/6-311 G+(d) in the Gaussian program. The permitted approaching angle between the x-axis and the plane consisting of O, N, F, and ϕ plays a key role to restrict the reaction of NO_2 and F_2 compared to the reaction of NO and F_2. This restriction in the reaction space is considered to be the main cause of different rate coefficients depending on the selection of $x = 1$ or 2 of the reaction of $F_2 + NO_x \rightarrow F + FNO_x$, which was also confirmed by the difference in Si etch rate using the F formed by those reactions.

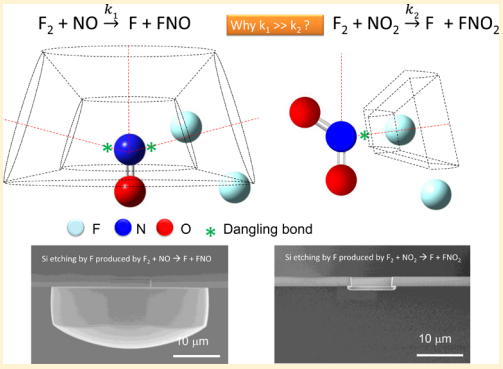

Generation of F in the gas phase is necessary to fabricate Si-based semiconductor devices and MEMS devices.[1−4] Various gases such as XeF_2[5−8] and ClF_3[9−14] have been reported to produce F and they have been used as precursors for the chemical dry etching apparatus to texture the Si single crystal solar panels[15] and to remove the Si layer activating the microelectromechanical systems (MEMS).[16] Recently, we reported that chemical reaction of F_2 and NO can be used to exothermically generate F.[17,18] Experimentally, several rate coefficients k_1 for the reaction (1) have been reported and representative values are listed in eqs (2)[19] and (2′).[20] Based on our previous calculation, the spontaneous reaction (1) would be expected without having a potential barrier.[17] Therefore, we believe the k_1 can be determined by eq (2′).

$$F_2 + NO \xrightarrow{k_1} F + FNO \quad (1)$$

$$k_1[\mathrm{cm^3/molecules{\cdot}s}] = 7.01 \times 10^{-13} \exp(-9.56 \times 10^3[\mathrm{J/mol}]/R[\mathrm{J/mol{\cdot}K}]T[\mathrm{K}]) \quad (2)$$

$$k_1[\mathrm{cm^3/molecules{\cdot}s}] = 1.1 \times 10^{-14} \text{ at } 315\ \mathrm{K} \quad (2')$$

where R is the gas constant (8.314 J/mol·K), and T is the temperature in the gas phase in Kelvin. The reaction of F_2 and NO_2 gases could also produce F by the reaction (3) with the rate coefficient expressed in eq (4).[21]

$$F_2 + NO_2 \xrightarrow{k_2} F + FNO_2 \quad (3)$$

$$k_2[\mathrm{cm^3/molecules{\cdot}s}] = 2.64 \times 10^{-12} \exp(-43.81 \times 10^3[\mathrm{J/mol}]/R[\mathrm{J/mol{\cdot}K}]T[\mathrm{K}]) \quad (4)$$

The activation energy of this reaction would be 0.45 eV at 298 K.[21] k_1 and k_2 from eqs (2), (2′), and (4) are plotted with respect to the temperature in Figure 1. The rate coefficient of k_1 is insensitive to the change in T whereas k_2 is strongly

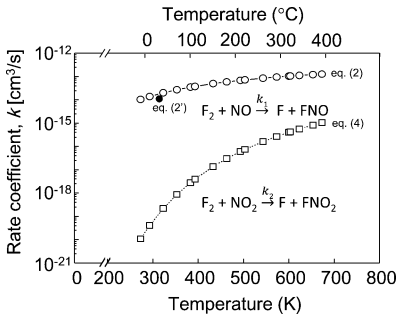

Figure 1. Relationships between the rate coefficient and the temperature of four reactions; i.e.; $F_2 + NO \xrightarrow{k_1} F + FNO$ and $F_2 + NO_2 \xrightarrow{k_2} FNO_2 + F$. Values of k_1 and k_2 were calculated by eqs 2 (plotted as ○), 2′ (plotted as ●), and 4 (plotted as □).

Received: October 30, 2014
Revised: December 28, 2014

DOI: 10.1021/jp510886b
J. Phys. Chem. A XXXX, XXX, XXX−XXX

Table 1. Comparison of the Total Energy Variation by Two Different Calculation Methods (DFT CAM 6-311G+(d) vs CCSD/cc-PVTZ)

total energy variation, ΔE (eV)	DFT CAM 6-311G+d (BSSE energy)	CC CCSD/cc-PVTZ	difference (CC-DFT)
F_2 + NO	0	0	0
F-FNO (n = 15)	−0.08	0.16	0.24
F-FNO (n = 30)	−1.31(0.03)	−0.91(0.09)	0.41
F + FNO	−1.16	−0.67	0.49
F_2 + NO_2	0	0	0
F-FNO_2 (n = 20)[a]	0.12	0.46	0.34
F-FNO_2 (n = 31)	−1.06(0.06)	−0.85	0.20
F + FNO_2	−0.99	−0.61	0.38

[a]Experimental value would be 0.45 eV.[20]

dependent on T. The cause of possessing different rate coefficients, k_1 and k_2, depending on the selection of x = 1 or 2 for the reaction of F_2 + NO_x → F + FNO_x has not been fully investigated yet. In this study, we evaluated the change in total energy and stereochemistry during the reaction of F_2 and NO_x to elucidate the cause of the difference in k_1 and k_2 by the density functional theory (DFT) with CAM-B3LYP/6-311G +(d)[22] in Gaussian 09.[23] Although the calculation results by CCSD/cc-PVTZ[24] would produce more accurate results as shown in Table 1, the computational time of CAM-B3LYP/6-311G+(d) was less than 1/10 than that of CCSD/cc-PVTZ. CAM-B3LYP/6-311G+(d) was employed as a first estimation to calculate the reaction space in this study since this function could predict the potential curve by adding 0.24−0.49 eV to the results calculated by CCSD/cc-PVTZ.

To calculate the allowable space of F_2 with respect to NO_x to initiate the reaction of F_2 + NO_x → F + FNO_x, Cartesian and polar coordinates were defined as shown in Figures 2(a) and 2(b) for x = 1 and 2, respectively. The position of F with respect to N was expressed in terms of (r, θ, ϕ) where the r was the distance between F and N, the θ was the angle between the z-axis and F−N, which was the same as 180° − ∠ONF, and the ϕ was the angle between the x-axis and the plane consisting of O, N, and F. The position of F with respect to F could be expressed in terms of r' and θ' where r' was the distance between F and F and θ' was the angle between FNN (∠FNN).

The first set of calculations, identified as calculation A, determined the change in total energies during the reaction of F_2 + NO_x → F−FNO_x → F + FNO_x. The r was reduced from 3.0 to 1.5 Å every 0.05 Å while arbitrarily choosing θ, ϕ, r', and θ' to obtain the chemical bonding structure of F−FNO_x that had the minimum total energy. Then, r' was increased in the increment of 0.05 Å until it became more than 2.5 Å, which implied the existence of no chemical bond between F and FNO_x. To obtain the baseline of the change in the chemical bonding structure, the total energies of F_2 and NO_x were calculated separately and the sum of those values were defined as 0 eV. The total energy calculation step at different r and/or r' was defined as a reaction step, n, and expressed as an integer. The difference in total energies at the beginning and the end of the reaction F_2 + NO_x → F−FNO_x → F + FNO_x was plotted as a total energy variation, ΔE, with respect to the n. To evaluate the stability of F−FNO_x at the lowest ΔE, the basis-set superposition error (BSSE) was calculated using the counterpoise method and the results are listed in Table 1.

The second set ΔE calculations, identified as calculation B, were designed to estimate the allowable reaction space of F_2 with respect to NO_x that can exothermically produce F.

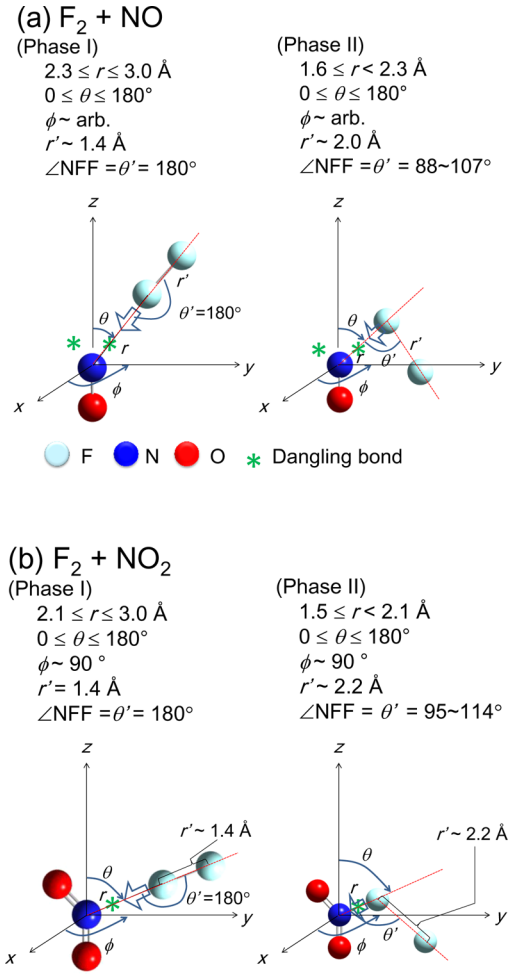

Figure 2. Reaction coordinates of (a) F_2 + NO ((i) ∠NFF = 180° in Phase I and (ii) ∠NFF < 180° in Phase II) and (b) F_2 + NO_2 ((i) ∠NFF = 180° in Phase I and (ii) ∠NFF < 180° in Phase II).

Constant r was chosen (r = 1.6, 1.7, 1.8, 1.9, 2.0, 2.3, 2.4, 2.6, 2.8, and 3.0 Å) and θ was varied from 0° to 180° for each r to obtain the F−FNO_x structure that had minimum total energy. The value of ϕ was set at 90° to calculate the dependence of ΔE with respect to r and θ and values of r' and θ' were selected from the results of calculation A at each selection of r. Once the minimum ΔE was calculated at the selected values of r and θ, ϕ was varied from 0 to 360° to evaluate the relationship between ΔE and ϕ.

DOI: 10.1021/jp510886b
J. Phys. Chem. A XXXX, XXX, XXX−XXX

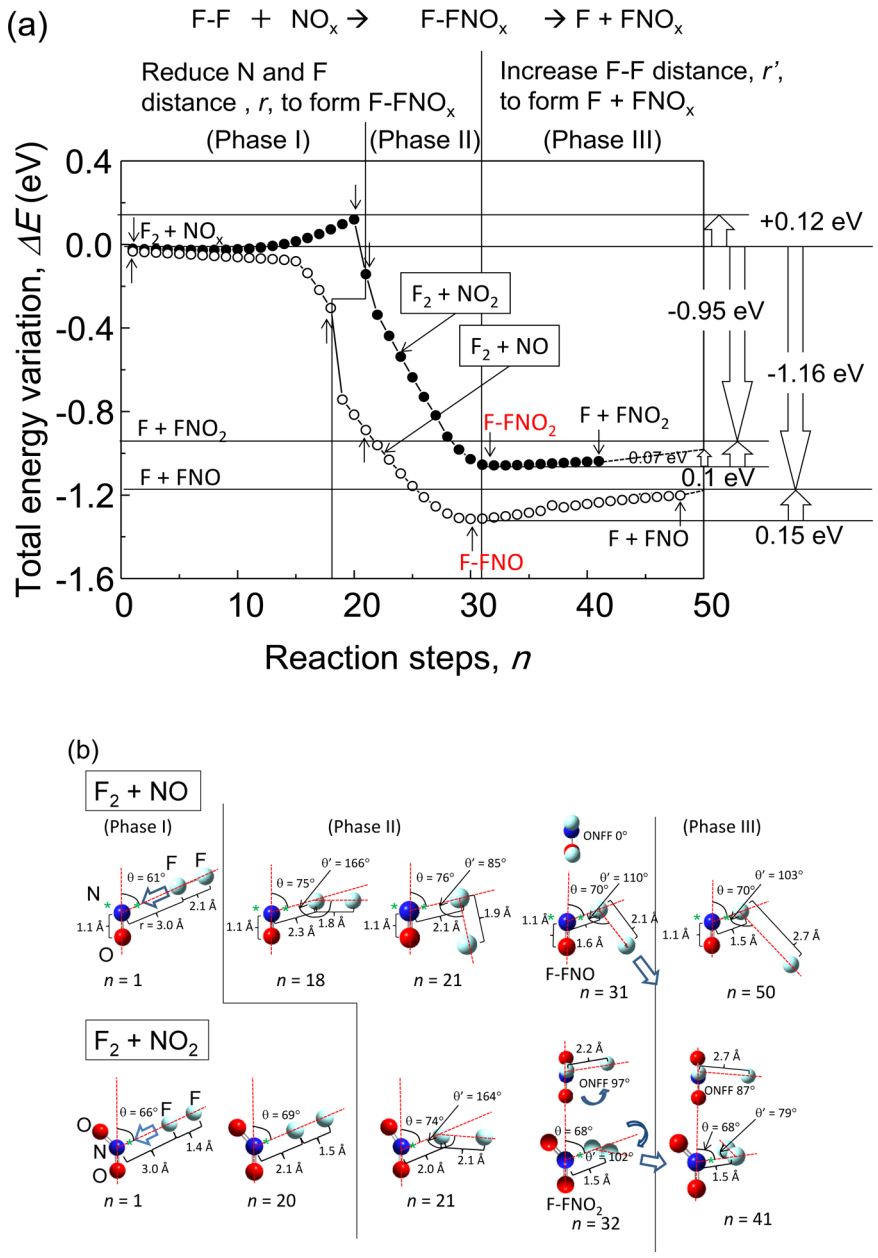

Figure 3. (a) The total energy variation of $F_2 + NO_x$ (x = 1 or 2) → F−FNO_x → F + FNO_x calculated by B3LYP/CAM 6-311+G(d) in Gaussian 09. (b) The list of chemical bonding structures at different reaction steps, n, in (a).

The results of calculation A are summarized in Figure 3. Figure 3a shows the change in ΔE with respect to the n during the reaction of $F_2 + NO_x$ → F−FNO_x → F + FNO_x and Figure 3b shows the corresponding chemical bonding structures during the reaction. When r was reduced from 3.0 to 2.3 Å for x = 1 and to 2.0 Å for x = 2, the θ' remained at ∼180° (labeled as "Phase I" in Figures 3(a) and 3(b)). No activation energy was present during the exothermic reaction of F_2 + NO → F−FNO. However, the reaction of $F_2 + NO_2$ → F−FNO_2 required 0.12 eV of activation energy based on the calculation. The presence of activation energy in reaction 3 is due to the presence of the long-range columbic repulsive force acting between O and F. The activation energy could be calculated more accurately with CCSD/cc-PVTZ at 0.46 eV where the experimental value is 0.45 eV[20] as shown in Table 1. CAM-B3LYP/6-311G+(d) underestimated this value by −0.33 eV. The total energy of F−FNO_x reduced significantly at around r ≈ 2.0 Å and θ' decreased from 180° (labeled as "Phase II" in Figures 3(a) and 3(b)) since the attractive force between N and F overcame the repulsive force between two O and F. ΔE became the minimum at r ≈ 1.5 Å with r' ≈ 2.0 Å for both x = 1 and 2 and the dihedral angle of ONFF was 0° for x = 1 whereas it was 97° for x = 2. When the F_2 and NO reaction occurs, an attractive force between N and F, and the repulsive force between O and F must be considered. Also, one F of F_2 must be located on the opposite side with respect to the lone pair of N. Therefore, the dihedral angle of ONFF became 0°. On the contrary, during the reaction between F_2 and NO_2, the attractive force between N and F, and the repulsive force between two O and F must be considered. Therefore, the dihedral angle of ONFF became close to 90°.

After the F−FNO_x was formed, the reaction of F−FNO_x → F + FNO_x was calculated by increasing r' from 2.0 Å to >2.5 Å. The slight increase of ΔE was observed during this reaction

DOI: 10.1021/jp510886b
J. Phys. Chem. A XXXX, XXX, XXX−XXX

(identified as "Phase III" in Figures 3(a) and 3(b)). This procedure simulated the endothermic reaction of F−FNO_x → F + FNO_x requiring ΔE of 0.1 to ∼0.15 eV. The energies released during the reaction of F_2 + NO_x → F−FNO_x (1.31 eV for x = 1 and 1.06 eV for x = 2) in Phases I and II were sufficient enough to initiate the endothermic reaction of F−FNO_x → F + FNO_x in Phase III. During Phase III, r and θ' did not change significantly. The differences in bond energies of F + FNO and F + FNO_2 were 0.2 eV. The calculated ΔE_F was 0.8 eV for x = 1 and 0.7 eV for x = 2. This result indicated that the bond energy of F + FNO and the energy that F possessed after the reaction of F_2 and NO_x are almost the same by the selection of x = 1 and 2.

Next, the allowable reaction space between F_2 and NO_x was calculated by changing r and θ during Phases I and II in Figure 3. From the calculation A results shown in Figure 3(a), F was produced exothermically when the differences in potential energies between F_2 + NO_x and F−FNO_x were more than 0.15 and 0.10 eV with x = 1 and 2, respectively. During Phase I, r was varied from 2.4 to 3.0 Å for x = 1 and 2.1 to 3.0 Å for x = 2 while fixing r' at 1.4 Å and θ' at 180°. During Phase II, r was varied from 1.6 to 2.3 Å for x = 1 and 1.5 to 2.0 Å for x = 2 while choosing r' at 1.8−2.0 Å and θ' at 85−117° for x = 1 and r' at 2.0−2.3 Å and θ' at 93−113° for x = 2. r' and θ' values were extracted from the results of calculation A with each r. ΔE was plotted with respect to the change in θ between 0 and 180° with the increment of 5°.

Figures 4(a) and 4(b) show ranges of r and θ that allowed the exothermic reaction of F_2 + NO → F−FNO or F_2 + NO → F−FNO → F + FNO during Phase I and Phase II, respectively. From Figure 4(a), NO and F_2 could exothermically react only when θ = 37−97° at r = 2.4−3.0 Å. The energy released from this reaction was less than 0.15 eV, which was not sufficient to initiate the endothermic reaction of F−FNO → F + FNO requiring more than 0.15 eV. Therefore, F would not be produced during Phase I. During Phase II, NO and F_2 may react exothermically to form F−FNO when $1.6 \le r \le 2.3$ Å and $38 \le \theta \le 107°$ as shown in Figure 4(b). Furthermore, the reaction of F_2 + NO → F−FNO → F + FNO would be expected at $1.6 \le r \le 2.3$ Å and $41° \le \theta \le 104°$ from Figure 4(b). From these results, ΔE became minimum when $r \approx 1.6$ Å and $\theta \approx 75°$. These calculation results are independent of the value of ϕ, which indicated that F_2 could approach N from $0 \le \phi \le 360°$.

Similarly, Figures 5(a) and 5(b) show the range of r and θ that allowed the exothermic reaction of F_2 + NO_2 → F−FNO_2 or F_2 + NO_2 → F−FNO_2 → F + FNO_2 during Phase I and Phase II, respectively. From Figure 5(a), the repulsion force acted between F and NO_2 by the reduction of r from 3.0 to 2.2 Å so that the allowable exothermic reaction space expressed in terms of θ was reduced significantly. This is the cause of the presence of the activation energy observed in Figure 3(a). The energy released from the reaction of F_2 + NO_2 → F−FNO_2 in Phase I was less than 0.10 eV. Therefore, the F generation would not be expected during Phase I. When r became less than 1.8 Å during Phase II, the attractive force acted between F and N so that the ΔE reduced significantly as shown in Figure 5(b). The energy released from the reaction of F_2 + NO_2 → F−FNO_2 became more than 0.1 eV at $1.5 \le r \le 1.8$ Å and $47° \le \theta \le 94°$ so that the reaction of F−FNO_2 → F + FNO_2 would be expected at this condition. ΔE was the minimum at $r \approx 1.5$ Å and $\theta \approx 69°$. Figure 5(c) shows the range of ϕ when the rest of the parameters were fixed at r of 1.5−1.8 Å, $\theta \approx 69°$. The

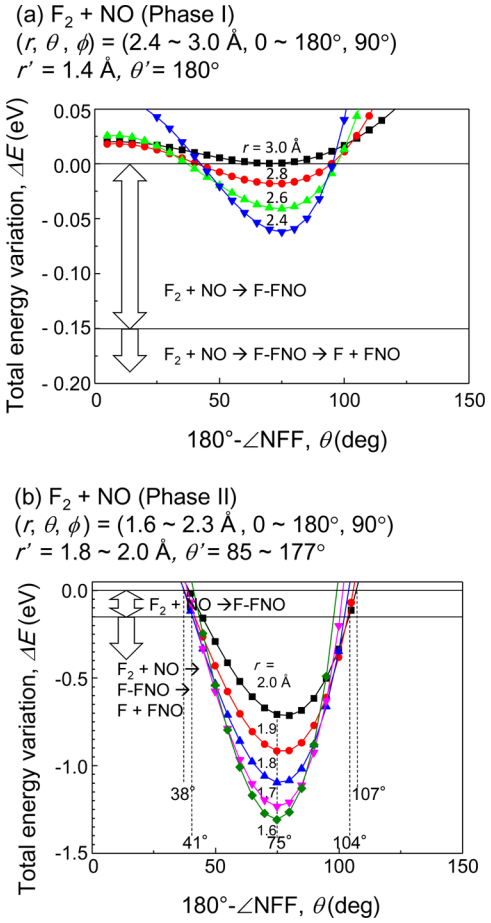

Figure 4. Total energy variation during the reaction of F_2 + NO → F−FNO → F + FNO when the F position with respect to N was changed by varying the F−N distance, r, and the angle between the z-axis and F−N, θ. Selected geometries for the calculations were (a) (r, θ, ϕ, r', θ') = (2.4−3.0 Å, 0−180°, 90°, 1.4 Å, 180°) that describe the F position with respect to N during Phase I in Figure 3, and (b) (r, θ, ϕ, r', θ') = (1.6−2.3 Å, 0−180°, 90°, 1.8−2.0 Å, 85−177°) that simulate the F position with respect to N in Phase II in Figure 3

corresponding r' and θ' for each r were selected from calculation A where r' and θ' are at 2.0−2.3 Å and 93° to ∼109°, respectively. The reaction of F_2 + NO_2 → F−FNO_2 → F + FNO_2 was allowed only at $42° \le \phi \le 138°$. ΔE was the minimum at $\phi \approx 90°$.

Based on the calculation results of Figures 4 and 5, the F generation by mixing F_2 and NO_x is allowable inside the region marked with the dotted line in Figure 6(a) for x = 1 and Figure 6(b) for x = 2. The reaction space was only defined by r and θ for x = 1 ($1.6 \le r \le 2.3$ Å and $41° \le \theta \le 104°$), whereas the reaction space was limited by r, θ, and ϕ for x = 2 ($1.5 \le r \le 1.8$ Å, $47° \le \theta \le 94°$, and $42° \le \phi \le 138°$) . The volume of the allowable reaction space shown in Figure 6(a) for F_2 + NO was ∼28 times larger than that of the reaction space shown in Figure 6(b) for F_2 + NO_2.

By comparing the change in ΔE and the allowable reaction space determined by varying r, θ, and ϕ during the reaction of F_2 + NO_x → F−FNO_x → F + FNO_x (x = 1 or 2) from Figures 3−6, we found several differences between the selection of x = 1 and 2. F_2 + NO → F−FNO is exothermic requiring no activation energy whereas the activation energy of 0.12 eV is necessary to initiate the reaction of F_2 + NO_2 → F−FNO_2. The allowable reaction space of F_2 + NO_2 → F−FNO_2 → F +

DOI: 10.1021/jp510886b
J. Phys. Chem. A XXXX, XXX, XXX−XXX

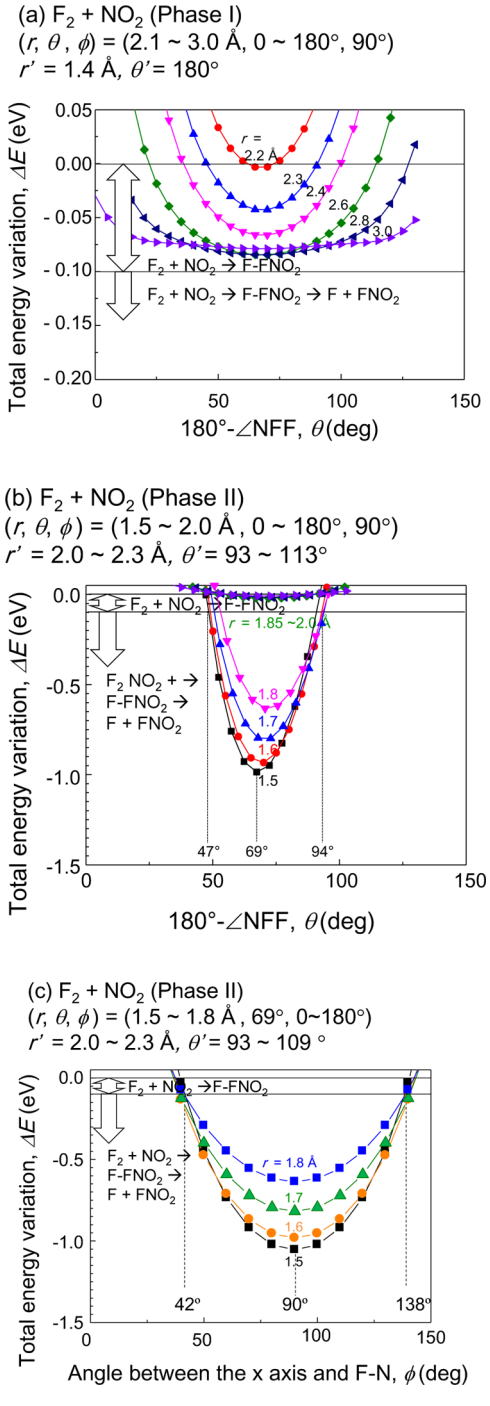

Figure 5. Total energy variation during the reaction of $F_2 + NO_2 \rightarrow F{-}FNO_2 \rightarrow F + FNO_2$ when the F position with respect to N was changed by varying the F−N distance, r, and the angle between the z-axis and F−N, θ. Selected geometries for the calculations were (a) (r, θ, ϕ, r', θ') = (2.1−3.0 Å, 0−180°, 90°, 1.4 Å, 180°) that describe the F position with respect to N during phase I in Figure 3, and (b) (r, θ, ϕ, r', θ') = (1.5−2.0 Å, 0−180°, 90°, 2.0−2.3 Å, 93−113°) that simulate the F position with respect to N in Phase II in Figure 3. (c) The allowable reaction space with respect to ϕ was calculated at the condition of (r, θ, ϕ, r', θ') = (1.5−1.8 Å, 69°, 0−180°, 2.0−2.3 Å, 93−109°) that simulate the F position with respect to N in Phase II in Figure 3.

FNO_2 was limited due to the presence of two O that restrict r, θ, and ϕ. We considered that this reaction space restriction

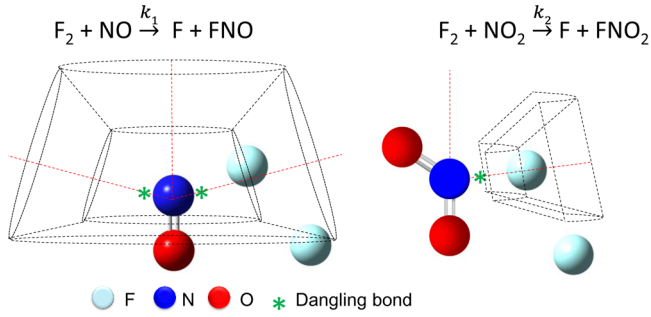

Figure 6. Allowable reaction space of F_2 and NO_x. F_2 may exothermically react to form F by the reaction of $F_2 + NO_x \rightarrow F{-}FNO_x \rightarrow F + FNO_x$ when F_2 approached inside the dotted line near N of NO_x (x = 1 or 2).

would lead to the significant change in k_1 and k_2 shown in Figure 1.

The evidence of $k_1 \gg k_2$ can be evaluated empirically by measuring the Si etch rate, which was calculated from the cross-sectional scanning electron microscope images of the etched Si depth divided by the F_2 and NO_x exposure time. The detailed Si etching experimental procedure was described elsewhere,[17,18] but briefly, a total of 109 sccm of Ar/F_2 + Ar/NO was introduced into the Pyrex tube while maintaining the pressure at 600 Pa and the substrate heating temperature at 27−350 °C. A p-type Si(100) sample with the resistivity of ∼1000 Ω cm and a 1 μm thick SiO_2 mask with 8 μm × 8 μm square openings, which was fabricated by the plasma enhanced chemical vapor deposition (PECVD) of tetraethylorthosilicate (TEOS $Si(OC_2H_5)_4$), was etched in the aforementioned Pyrex tube with the gas exposure time of 5−30 min.

Several assumptions were made to relate the measured Si etch rate to the F density in the gas phase. In our previous study, we considered the surface reaction between Si and molecules in the gas phase (F_2, NO, F, and FNO) and concluded that all of the molecules could react at the Si surface when the substrate temperature was low due to the presence of the adsorbed layer.[17,18] However, when the substrate heating temperature was ramped at above 230 °C, F becomes dominant to react with Si due to the loss of the adsorbed layer and the increase of F density by the Arrhenius law. The F density with respect to the temperature was also confirmed from the previous study by Ibbotson et al.[6] Therefore, we consider that the F flux is the sole contributor to explain the differences in etch rate of Si at the elevated substrate heating temperature in this study.

The 10% of F generated in the gas phase would contribute the Si etching and the 90% of F would be desorbed back to the gas phase.[25] We also assumed that all F_2 was consumed in the gas phase to generate F. The recombination of F at the Si surface to form F_2 would be negligibly small since the bond energy of Si−F (6.12 eV)[26] is much higher than that of F−F (1.64 eV).[26] The contribution of NO and NO_2 to the Si dangling bond passivation (calculated bond energies of Si_9H_{13}−NO_x (x = 1, 2) are 0.9 eV[18] and 0.8 eV[27]) would mainly occur at the substrate heating temperature, T, at below 230 °C.[18] Bond energies of Si_9H_{13}−FNO and Si_9H_{13}−FNO_2 would be 4.4 eV[18] and 1.1 eV[27] and they were lower than the bond energies of Si_9H_{13}−F (5.7 eV)[18] so that F would be the main reactant at the Si surface. Therefore, the Si etch rate could be related only to the F density when the substrate heating temperature was increased to >230 °C.

DOI: 10.1021/jp510886b
J. Phys. Chem. A XXXX, XXX, XXX−XXX

The comparison of the Si etch rate in F_2 and NO_x is shown in Figure 7. The representative cross-sectional images of etched

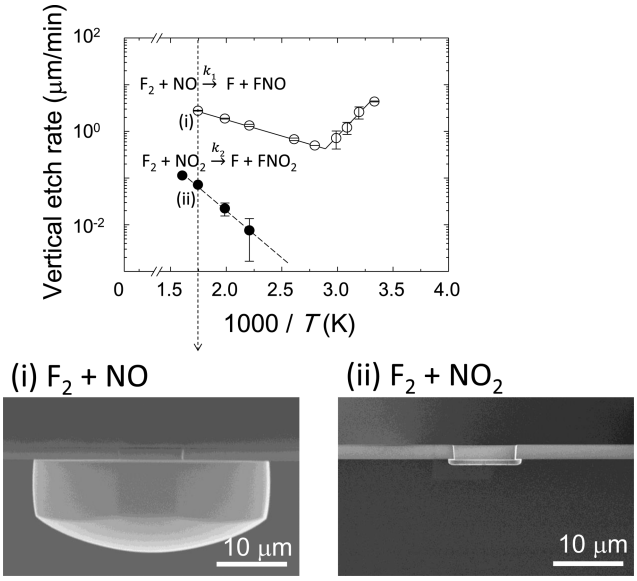

Figure 7. Relationship between the Si etch rate and the substrate temperature. The cross-sectional scanning electron microscope images of the patterned Si in F_2 + NO and F_2 + NO_2 at 300 °C are also shown.

Si are also given when the substrate heating temperature was set at 300 °C. The measured Si etch rate in F_2 and NO was ~30 times faster than that in F_2 and NO_2 at >230 °C as shown in Figure 7. This value was the same magnitude as the reaction space volume calculated in Figure 6. Based on these findings, we can calculate that the first estimation of the difference in k_1 and k_2 could be made by the proposed stereochemistry calculation using the DFT that was employed in this study.

In summary, the causes of the difference of the rate constant of the reactions of F_2 + NO → F + FNO and F_2 + NO_2 → F + FNO_2 were evaluated by using the DFT calculation. We found that generation of F was more difficult in F_2 and NO_2 than in F_2 and NO since the F_2 + NO_2 → F−FNO_2 required activation energy and the presence of two O bonded to N restricts the F_2 reaction space with respect to NO_2. The significant difference in the rate constant by the selection of NO or NO_2 could be estimated by the proposed streochemical arrangement in this study.

AUTHOR INFORMATION

Corresponding Author

*Tel +81-80-2348-8900. E-mail: stajima@plasma.engg.nagoya-u.ac.jp.

Notes

The authors declare no competing financial interest.

ACKNOWLEDGMENTS

We greatly acknowledge the research support funding provided by Tatematsu Zaidan, Aichi, Japan, JST A-step seeds validation, feasibility study stage, JSPS KAKENHI Grant Nos. 25600123 and 26706022, and Sumitomo Seika Chemicals Co, Ltd. S.T. thanks Dr. Satoru Iuchi for the variable discussion and comments.

REFERENCES

(1) Mucha, J. A.; Donnelly, V. M.; Flamm, D. L.; Webb, L. M. Chemiluminescence and the Reaction of Molecular Fluorine with Silicon. *J. Phys. Chem.* **1981**, *85*, 3529−3532.
(2) Flamm, D. L. Mechanisms of Silicon Etching in Fluorine- and Chlorine-Containing Plasmas. *Pure Appl. Chem.* **1990**, *62*, 1709−1720.
(3) Weakliem, P. C.; Carter, E. A. Surface chemical reactions studied via ab initio derived molecular dynamics simulations: Fluorine etching of Si(100). *J. Chem. Phys.* **1993**, *98*, 737−745.
(4) Lieberman, M. A.; Lichtenberg, A. J. *Principles of Plasma Discharges and Materials Processing*, 2nd ed.; John Wiley & Sons, Inc.: Hoboken, NJ, 2005; p 573.
(5) Coburn, J. W.; Winters, H. F. Ion and Electron Assisted Gas Surface Chemistry—An Important Effect in Plasma Etching. *J. Appl. Phys.* **1979**, *50*, 3189−3195.
(6) Ibbotson, D. E.; Flamm, D. M.; Mucha, J. A.; Donnelly, V. M. Comparison of XeF_2 and F atom Reactions with Si and SiO_2. *Appl. Phys. Lett.* **1984**, *44*, 1129−1131.
(7) Aliev, V. S.; Kruchinin, V. N. Development of Si(100) Surface Roughness at the Initial Stage of Etching in F_2 and XeF_2 Gases: Ellipsometric Study. *Surf. Sci.* **1999**, *442*, 206−214.
(8) Holt, J. R.; Hefty, R. C.; Tate, M. R.; Ceyer, S. T. Comparison of the Interactions of XeF_2 and F_2 with Si(100)2 × 1. *J. Phys. Chem. B* **2002**, *106*, 8399−8406.
(9) Ibbotson, D. E.; Mucha, J. A.; Flamm, D. L.; Cook, J. M. Plasmaless Dry Etching of Silicon with Fluorinecontaining Compounds. *J. Appl. Phys.* **1984**, *56*, 2939−2942.
(10) Saito, Y.; Yamaoka, O.; Yoshida, A. Plasmaless cleaning process of silicon surface using chlorine trifluoride. *Appl. Phys. Lett.* **1990**, *56*, 1119−1121.
(11) Saito, Y.; Yamaoka, O.; Yoshida, A. Plasmaless Etching of Silicon using Chlorine Trifluoride. *J. Vac. Sci. Technol. B* **1991**, *9*, 2503−2506.
(12) Kim, H. M.; Shibuya, M.; Yoshida, A.; Kitagawa, M. Gas-Phase Etching with ClF_3 Gas at Atmospheric Pressure and at Room Temperature − Anisotropic Etching. *Appl. Surf. Sci.* **1998**, *133*, 1−4.
(13) Saito, Y. Characteristics of Plasmaless Dry Etching of Silicon-Related Materials using Chlorine Trifluoride Gas. *Sens. Mater.* **2002**, *14*, 231−237.
(14) Seki, T.; Yoshino, T.; Senoo, T.; Koike, K.; Ninomiya, S.; Aoki, T.; Matsuo, J. High Speed Si Etching with ClF_3 Cluster Injection. *AIP Conf. Proc.* **2010**, *1321*, 317−320.
(15) Matsui, T.; Tsukiji, M.; Saika, H.; Toyama, T.; Okamoto, H. Influence of substrate texture on microstructure and photovoltaic performances of thin film polycrystalline silicon solar cells. *J. Non-Cryst. Solids* **2002**, *299−302*, 1152−1156.
(16) Xu, D.; Xiong, B.; Wu, G.; Wang, Y.; Sun, X.; Wang, Y. Isotropic Silicon Etching With XeF2 Gas for Wafer-Level Micromachining Applications. *J. Microelectromech. Syst.* **2012**, *21*, 1436−1444.
(17) Tajima, S.; Hayashi, T.; Ishikawa, K.; Sekine, M.; Hori, M. Room-Temperature Si Etching in NO/F_2 Gases and the Investigation of Surface Reaction Mechanisms. *J. Phys. Chem. C* **2013**, *117*, 5118−5125.
(18) Tajima, S.; Hayashi, T.; Ishikawa, K.; Sekine, M.; Hori, M. Formation of Nanoporous Features, Flat Surfaces, or Crystallographically Oriented Etched Profiles by the Si Chemical Dry Etching Using the Reaction of F_2 + NO → F + FNO at an Elevated Temperature. *J. Phys. Chem. C* **2013**, *117*, 20810−20818.
(19) Kolb, C. E. Resonance fluorescence study of the gas phase reaction rate of nitric oxide with molecular fluorine. *J. Chem. Phys.* **1976**, *64*, 3087−3090.
(20) Orkin, V. L.; Chaikin, A. M. Determination of the rate constants for formation of fluorine atoms in the reaction of molecular fluorine with NO, C_2H_4, and C_2F_4. *Kinet. Catal.* **1982**, *23*, 438−442.
(21) Perrine, R. L.; Johnston, H. S. Kinetics of the Fast Reaction between Nitrogen Dioxide and Fluorine. *J. Chem. Phys.* **1953**, *21*, 2202−2205.
(22) Yanai, T.; Tew, D. P.; Handy, N. C. A New Hybrid Exchange-Correlation Functional using the Coulomb-Attenuating Method (CAM-B3LYP). *Chem. Phys. Lett.* **2004**, *393*, 51−57.

DOI: 10.1021/jp510886b
J. Phys. Chem. A XXXX, XXX, XXX−XXX

(23) A detailed description of Gaussian program is listed in http://www.gaussian.com/; accessed Jan 9, 2013.
(24) Sholl, D. S.; Steckel, J. A. *Density Functional Theory: A Practical Introduction*; John Wiley & Sons, Inc.: Hoboken, NJ, 2009; pp 23−27.
(25) Ninomiya, K.; Suzuki, K.; Nishimatsu, S.; Okada, O. Reaction of atomic fluorine with silicon. *J. Appl. Phys.* **1985**, *58*, 1177−1182.
(26) Pauling, L. *General Chemistry*; Dover: New York, NY, 1970; p 913.
(27) Tajima, S. the bond energy calculation of Si_9H_{13}-NO_2 and Si_9H_{13}-FNO_2 by the density functional theory (DFT) with CAM-B3LYP/6-311G+(d)[22] in *Gaussian 09*.[23] The calculation procedure was described in ref 18.

DOI: 10.1021/jp510886b
J. Phys. Chem. A XXXX, XXX, XXX−XXX